Electron-temperature-gradient-driven ion-scale turbulence in high-performance scenarios in Wendelstein 7-X

Alessandro Zocco [1], Linda Podavini [1,2], Felix Wilms [3], Alejandro Bañón Navarro [3], and Frank Jenko [3]

[1] *Max-Planck-Institut für Plasmaphysik, Wendelsteinstraße 1, D-17491 Greifswald, Germany*

[2] *Institut für Physik, Universität Greifswald, 17489 Greifswald, Germany*

[3] *Max-Planck-Institut für Plasmaphysik, Boltzmannstraße 2, 85748 Garching bei München, Germany*

(Received 15 May 2024; accepted 4 July 2024; published 24 July 2024)

Through intercode gyrokinetic numerical simulations, we predict that, for the conditions met during improved performances in the stellarator Wendelstein 7-X, turbulent transport can be dominated by electron-temperature-gradient-driven ion-scale electrostatic turbulence. We find that previously numerically observed large density-gradient-driven turbulence reductions must be attributed to the artificial suppression of the electron temperature gradient. Instead, when electrons have a finite temperature gradient, we observe a moderate turbulence suppression whose quantitative comparison with experimental findings remains challenging. In such partial suppression, the nonlinear dynamics of zonal flows plays a pivotal role as opposed to the underlying most unstable linear modes.

DOI: 10.1103/PhysRevResearch.6.033099

I. INTRODUCTION

Wendelstein 7-X (W7-X) is the most advanced modular optimized stellarator ever built [1]. It has been conceived to feature excellent magnetohydrodynamic stability and to avoid current-driven disruptive events. Additionally, it is equipped with an island divertor to investigate solutions to the power exhaust problem for a potential fusion reactor. Importantly, its magnetic field has been tailored to reduce collisional (neoclassical) transport [2]. While it has been demonstrated that this goal has been achieved [3], turbulence now limits the performance of W7-X. This highlights the need to understand and control turbulent transport in stellarators and provides additional opportunities for design optimization. In this context, recent experiments in W7-X exhibited a transient performance improvement related to peaked density profiles after the injection of frozen hydrogen pellets [4]. A possible explanation of this finding was put forward in Ref. [5], related to a change of the character of the underlying linear microinstabilities in the presence of a strong density gradient. Support for this claim was provided by gyrokinetic simulations which set the electron temperature gradient to 0. Since W7-X is a mostly electron-heated device with peaked electron temperature profiles, some important questions concerning the applicability of the simulation results have remained unanswered.

More generally speaking, with the exception of the work by Wilms *et al.* [6], turbulent energy transport properties of W7-X have usually been investigated via gyrokinetic simulations that either set the electron temperature gradient to 0 or neglect its role [7], while it is known for having an effect on particle transport [8,9]. In the present work, we investigate the role of finite electron temperature gradients on turbulent energy transport in W7-X, focusing on high-performance discharges. A series of studies are carried out with the gyrokinetic turbulence codes STELLA [10] and GENE [11]. We predict that in the presence of finite electron temperature gradients, turbulent energy fluxes on ion-gyroradius scales can be dominated by the electron channel. Moreover, we find that the previously reported turbulence suppression mechanism due to density peaking was overestimated due to the lack of inclusion of the true electron kinetics [5].

II. MODEL EQUATIONS AND NUMERICAL PARAMETERS

We consider turbulence associated with fluctuations of the electrostatic potential, φ, which satisfies the quasineutrality condition

$$\sum_s e_s \int d^3\mathbf{v} F_{0s} \frac{e_s \varphi}{T_{0s}} = \sum_s e_s \int d^3\mathbf{v} \sum_{\mathbf{k}} e^{i\mathbf{k}\cdot\mathbf{r}} J_0(a_s) \delta G_{s\mathbf{k}} \tag{1}$$

for species s with charge e_s and equilibrium temperature T_{0s}. The equilibrium distribution function F_{0s} is taken to be Maxwellian with the total density $n_s = \int d^3\mathbf{v} f_s$. Here $f_s = F_{0s} + \delta f_s \equiv F_{0s}(1 - e_s\varphi(\mathbf{r},t)/T_{0s}) + \delta G_s(\mathbf{R}_s, \mu, \mathcal{E}, t) + \mathcal{O}(\epsilon^2)$, and $\delta f_s/F_{0s} \sim \epsilon \sim k_\parallel/k_\perp \sim \rho_* \equiv \epsilon \ll 1$, where $k_\parallel$ and $k_\perp$ are wave vectors along and across the equilibrium magnetic field. $\mathbf{R}_s = \mathbf{r} + \mathbf{v}_\perp \times \hat{\mathbf{b}}/\Omega_s$ is the gyrocenter position, where $\mathbf{r}$ is the particle position, $\Omega_s = e_s B/(m_s c)$, $\hat{\mathbf{b}} = \mathbf{B}/B$, with $\mathbf{B}$ being the equilibrium magnetic field,

and $\mu = v_\perp^2/(2B)$ and $\mathcal{E} = v^2/2$ are the velocity space coordinates. The Bessel function $J_0 = J_0(a_s)$, with $a_s = 2B\mu k_\perp^2/\Omega_s^2$, relates the Fourier transform of δG_s with respect to $\mathbf{R}_s$ to its Fourier transform with respect to $\mathbf{r}$. The function δG_s satisfies the nonlinear gyrokinetic equation [12]

$$\left(\frac{\partial}{\partial t} + v_\parallel \nabla_\parallel + \mathbf{v}_{d,s}\cdot\nabla\right)\delta G_s = \frac{e_s F_{0s}}{T_{0s}}\frac{\partial}{\partial t}\langle\varphi\rangle_{\mathbf{R}_s} - \frac{c}{B}\hat{\mathbf{b}}\cdot\nabla\langle\varphi\rangle_{\mathbf{R}_s}\times\nabla F_{0s} - \frac{c}{B}\hat{\mathbf{b}}\cdot\nabla\langle\varphi\rangle_{\mathbf{R}_s}\times\nabla\delta G, \quad (2)$$

where $\langle\varphi\rangle_{\mathbf{R}_s} = \sum_{\mathbf{k}}\langle\varphi\rangle_{\mathbf{R}_s,\mathbf{k}}\exp(i\mathbf{k}\cdot\mathbf{R}_s)$ with $\langle\varphi\rangle_{\mathbf{R}_s,\mathbf{k}} = J_0(a_s)\varphi_{\mathbf{k}}$ being the gyroaveraged electrostatic potential, $\nabla = \partial/\partial\mathbf{R}_s$, $\mathbf{v}_{d_s} = -v_\parallel\hat{\mathbf{b}}\times\nabla(v_\parallel/\Omega_s)$, and $v_\parallel = \pm\sqrt{2(\mathcal{E} - B\mu)}$.

We perform a series of numerical simulations with the gyrokinetic codes STELLA [10] and GENE [11]. We consider two kinetic particle species (ions and electrons) with equal temperatures at the radial location $r/a = 0.63$ for a standard geometric configuration of W7-X [5]. Here a is the average minor radius and $r = a\sqrt{\psi/\psi_{\rm LCFS}}$, where $\psi = \psi_t/(2\pi)$ with ψ_t being the toroidal magnetic flux, and $\psi_{\rm LCFS}$ is its value at the last closed flux surface. Flux-tube coordinates are used, and thus $\mathbf{B} = \nabla\alpha\times\nabla\psi$, where α labels field lines, z is a general toroidal angle which measures the distance along the magnetic field, and $\mathbf{k}_\perp = k_\psi\nabla\psi + k_\alpha\nabla\alpha$. Furthermore, $d\iota/ds = 1.181\times10^{-1}$, where $\iota = 0.89$ measures the pitch of the field lines. In all cases, the field-line-following domain for the variable z is centered at the outboard midplane of the "bean-shaped" poloidal cross section, extending for slightly less than two poloidal turns. It is thus nearly twice as long as the domain customarily used [5], allowing for a more effective turbulence field-line decorrelation. Specifically, we simulate 11 field periods, with the equilibrium field's period being 5. The number of points in the z direction is either $n_z = 100$ or $n_z = 150$ for nonlinear runs. The velocity space resolution is $n_\mu = 24$ with $l_\mu = [0, 9]$ and $n_{v_\parallel} = 46$ with $l_{v_\parallel} = [-3, 3]$. For our set of simulations, we use two reference cases [5], one with moderate gradients [ECR case, $(a/L_n, a/L_{Ti}) = (0.8, 2.5)$] and one representing pellets' enhanced performance scenarios [PEP case, $(a/L_n, a/L_{Ti}) = (3.0, 4.5)$]. Here, $a/L_Q = Q^{-1}dQ/d\psi$ is a suitably normalized characteristic gradient scale length. Both cases are run with finite and zero electron temperature gradients, $a/L_{T_e} = a/L_{T_i}$ and $a/L_{T_e} = 0$, respectively. We employ $\rho_i k_y^{\rm min} = 0.05$; the number of points in the (radial) $x = dx/d\psi(\psi - \psi_0)$ direction is $n_x = 179$. While, linearly, in the $y = dy/d\alpha(\alpha - \alpha_0)$ direction, we can easily resolve the electron scales, nonlinearly we devised a procedure to evaluate ion-scale turbulent energy fluxes in a reliable and yet affordable way. Anticipating that the PEP case with $\nabla T_e = \nabla T_i$ would manifest a maximum growth rate for $k_y\rho_i \approx 4$, we first performed a large nonlinear simulation that would capture all the relevant linear scales. We then reduced the k_y domain, monitoring acceptable changes in the nonlinear heat flux. Similar values are used for the GENE simulations.

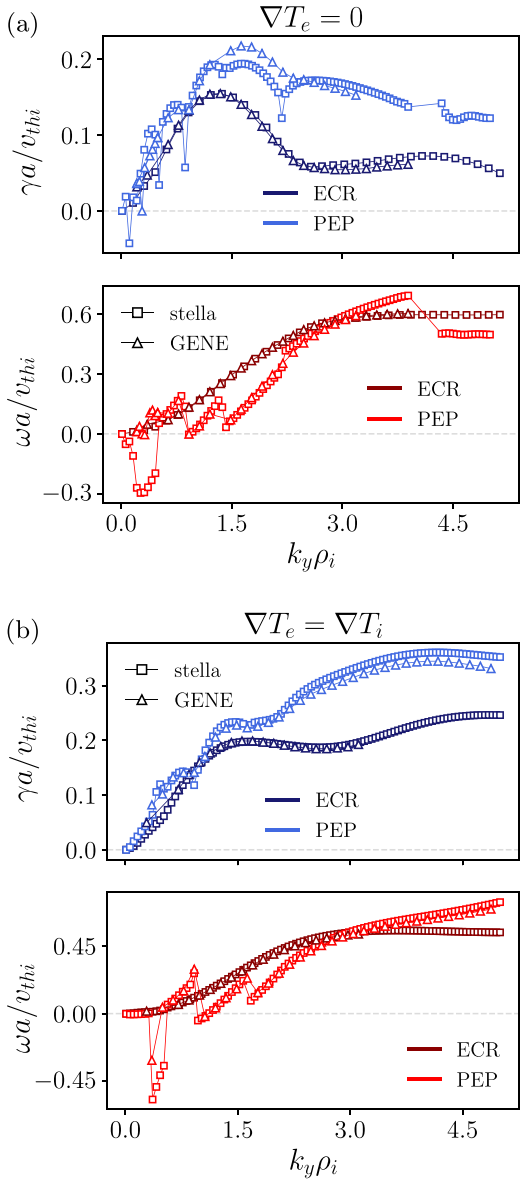

FIG. 1. W7-X linear spectra for $\nabla T_e = 0$ and $\nabla T_e = \nabla T_i$, $k_x\rho_i = 0$, as obtained from the STELLA and GENE codes. Positive $\omega a/v_{\rm thi}$ indicates mode propagation in the ion diamagnetic direction.

III. LINEAR MICROINSTABILITIES

The wave-number spectra of the resulting linear microinstabilities (for $k_x\rho_i = 0$) are shown in Figs. 1(a) and 1(b). The respective linear simulations are performed using the same flux-tube length as the nonlinear ones. The purpose of this choice is to guarantee a one-to-one correspondence between the active modes in the linear stage of the nonlinear calculation (initialized at small amplitudes) and the linear modes shown here. Thus, its length is set to allow sufficient turbulence decorrelation, *nonlinearly*. As can be seen, the agreement between STELLA and GENE is excellent, except some tolerable discrepancies for the $\nabla T_e = 0$ ECR case, which will be virtually irrelevant in setting the levels of energy fluxes. For zero electron temperature gradients [Fig. 1(a)], the transition to the shorter-wavelength, more

TABLE I. Time-averaged turbulent energy fluxes in gyro-Bohm units. GENE results are shown in parentheses.

	ECR	PEP	∇T_e
Q_i	9.42(10.18)	2.82 (2.03)	0
Q_e	0.93 (1.02)	0.87 (0.60)	0
Q_i	4.16 (4.60)	2.35	∇T_i
Q_e	1.90 (2.39)	4.07	∇T_i

stable ion-driven trapped electron mode (iTEM) [13,14] of Fig 4(b) of Ref. [5] is not observed. Instead, the PEP case is generally *more* unstable *at all* wavelengths. In particular, a long-wavelength electron mode is destabilized [13,15–17]. The inclusion of a finite electron temperature gradient changes the linear picture completely, as can be seen in Fig. 1(b). The ECR case still shows the typical long- and short-wavelength ion-temperature-gradient-driven modes spectra of Gao *et al.* [18–20], but now dominated by the short-wavelength branch [17,21]. This situation has been studied, even nonlinearly, in tokamaks [19]. A finite electron temperature gradient has a *destabilizing* effect on the PEP case as well, showing a maximum growth rate at $k_y\rho_i = 4$. We conclude that the destabilizing action of the increased temperature gradient is sufficiently large that it exceeds the stabilization associated with the density gradient, casting doubt on the explanation of the mechanism for enhanced performance of W7-X put forward in Ref. [5].

IV. NONLINEAR SIMULATION RESULTS

In Fig. 2, we display the time traces of the turbulent electron and ion energy fluxes in gyro-Bohm units, $Q_s = \hat{Q}_s/Q_{\rm gB}$, with $\hat{Q}_s = 0.5\int(dl/B)\int d^3\mathbf{v}v^2\delta f_s\mathbf{v}_E\cdot\nabla x$ and $Q_{\rm gB} = n_{\rm ref}T_{\rm ref}v_{\rm thi}\rho_i^2/a^2$. Here, we use $T_{\rm ref}^{\rm ECR} = 0.8$ keV, $T_{\rm ref}^{\rm PEP} = 1.5$ keV, $n_{\rm ref}^{\rm ECR} = 2.8\times10^{19}$ m^{-3}, and $n_{\rm ref}^{\rm ECR} = 4.9\times10^{19}$ m^{-3}, and $\mathbf{v}_E = c/B^2\nabla\varphi\times\mathbf{B}$ is the fluctuating $\mathbf{E}\times\mathbf{B}$ drift. The time-averaged turbulent fluxes are summarized in Table I. In the ECR case, the inclusion of a finite electron temperature gradient causes a significant increase/decrease in the electron/ion channel. The ion channel still dominates the total energy flux, but Q_i/Q_e drops from ∼10 to ∼2. In the PEP case, the inclusion of a finite electron temperature gradient has even more significant consequences: The *electron* channel now dominates, providing ∼60% of the total energy flux. The realistic comparison of the ECR and PEP cases (with nonzero electron temperature gradients) unveils a different scenario, characterized by a moderate reduction/increase in the ion/electron channel, which results in the dominance of the electron channel in the PEP case.

To allow for a quantitative analysis, we introduce turbulent thermal diffusivities, $\chi_s = \overline{Q}_s/(\langle g^{xx}\rangle a/L_T)$, where $\overline{(\dots)}$ is a time average, $\langle\dots\rangle$ is a field-line average, and $g^{xx} = \nabla x\cdot\nabla x$. In S.I. units, we thus obtain the values displayed in Table II. In the presence of a finite electron temperature gradient, one finds $\chi_i^{\rm PEP}/\chi_i^{\rm ECR} = 0.80$, in contrast to $\chi_i^{\rm PEP}/\chi_i^{\rm ECR} = 0.43$ for $\nabla T_e = 0$. Meanwhile, the experimental values reported in Ref. [5] amount to $\chi_i^{\rm PEP}/\chi_i^{\rm ECR}\approx 0.25/0.7\approx 0.36$.

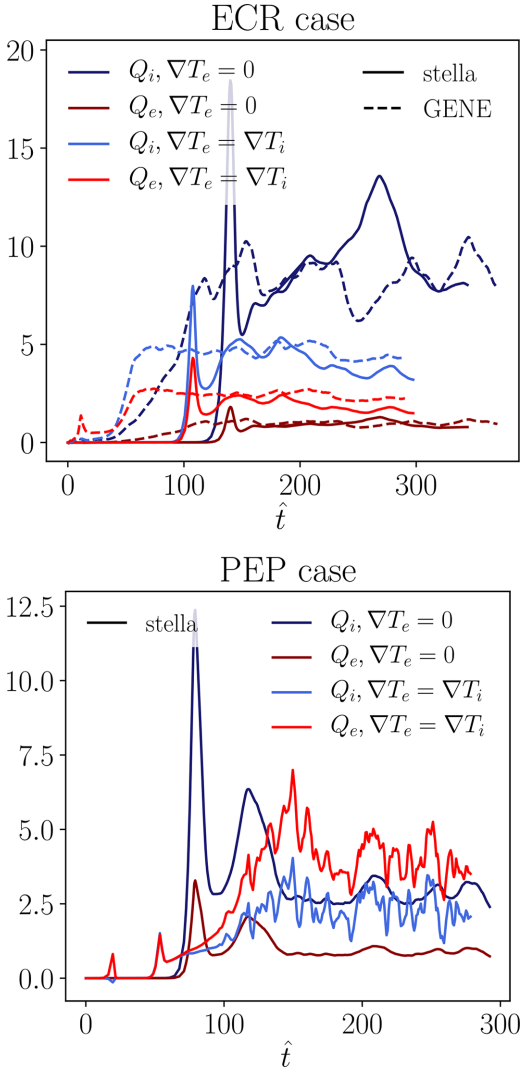

FIG. 2. Nonlinear energy flux traces in gyro-Bohm units, ECR and PEP cases, with and without ∇T_e. Here $\hat{t} = tv_{\rm thi}/a$.

Above, we argue that the linear considerations of Ref. [5] cannot explain the transition to improved performance in W7-X. Now, we inspect the wave-number spectra of the turbulent energy fluxes [Fig. (3)] and the time traces of (linearly and nonlinearly) dominant modes along with those of zonal ($k_y = 0$) modes. The nonlinear energy flux spectra show a slight increase at small scales. This is an indication of the fact that the *electron scale* transport channel (at really fine scales) is very likely not negligible. Its role in stellarators, however, needs further investigations, and whether it will affect the ion-scale turbulence levels is still an open question. The interaction between ion- and electron-scale turbulence can be extremely complicated [22–24], but the overall level of heat

TABLE II. Turbulent thermal diffusivities from STELLA in S.I. units.

Units, m^2/s	$\nabla T_e = 0$	$\nabla T_e = \nabla T_i$
$\chi_i^{\rm PEP}/\chi_i^{\rm ECR}$	2.50/5.88	2.08/2.60
$\chi_e^{\rm PEP}/\chi_e^{\rm ECR}$	N.A.	3.60/1.19

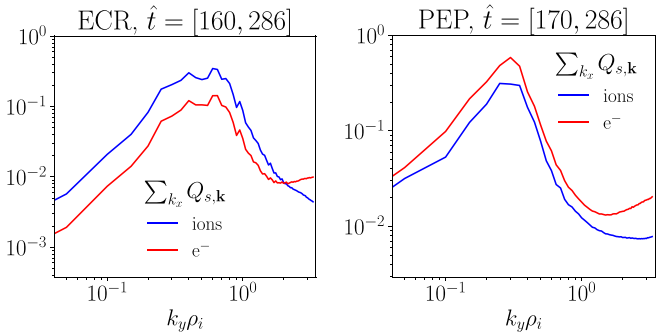

FIG. 3. Nonlinear energy flux spectra for W7-X with $\nabla T_e = \nabla T_i$: ECR and PEP cases. Time windows refer to the respective time traces.

transport *at the ion scale* (which is the one of interest in this work) can remain virtually unchanged if one performs a full scale *electrostatic* simulation or a properly truncated one [23]. This is, therefore, the working hypothesis behind the procedure for the choice of the k_y domain previously described. From the point of view of the evolution of the zonal flows, we observe that the key difference between the ECR and PEP case is that the latter shows a much stronger coupling between the zonal modes and the nonlinearly dominant scale ($k_y\rho_i \approx 0.4$, see Fig. 3) in the early nonlinear phase (PEP trace in Fig. 4, $t v_{\mathrm{thi}}/a = [60, 100]$). Electron and ion energy fluxes are virtually identical throughout the linear phase and this early nonlinear phase. After reaching the amplitude of the most unstable linear mode (notice that this instant can be determined unambiguously in all cases), the zonal flow undergoes a violent growth at $\hat{t} \approx 100$, the electron channel dominating over the ion one, which is now prone to a much more efficient zonal-flow stabilization than in the ECR case. Thus, for the PEP case, nearly all k_y scales are controlled by the zonal flow: $\sum_{k_x,k_y}\langle\varphi^2\rangle / \sum_{k_x}\langle\varphi^2\rangle_{k_y=0} \equiv \zeta \approx 0.8$. Notably, this is manifestly less evident for the ECR case, where $\zeta = 0.4$ (see also Fig. 4). Density gradient turbulence reduction is, therefore, due to this purely nonlinear dynamics just described, instead of the transition from the Ion Temperature Gradient driven mode to the ion-driven Trapped Electron Mode as previously suggested.

V. DISCUSSION AND CONCLUSION

Through a series of carefully designed studies with the gyrokinetic turbulence codes STELLA and GENE, we have investigated the impact of the finite electron temperature gradients in W7-X turbulent transport and also reassessed the transition to high performance scenarios. When electron temperature gradients are neglected, the increased density gradients associated with the latter seem to play a more substantial stabilizing role than in practice, in the reduction of turbulent transport [16]. When finite electron temperature gradients are also included, peaked-density discharges feature a linear wave-number spectrum of microinstabilities which is not compatible with the ones put forward in previous works aiming at explaining W7-X high performances through linear physics. The absence of the electron temperature gradient in numerical simulations causes an artificially high turbulence

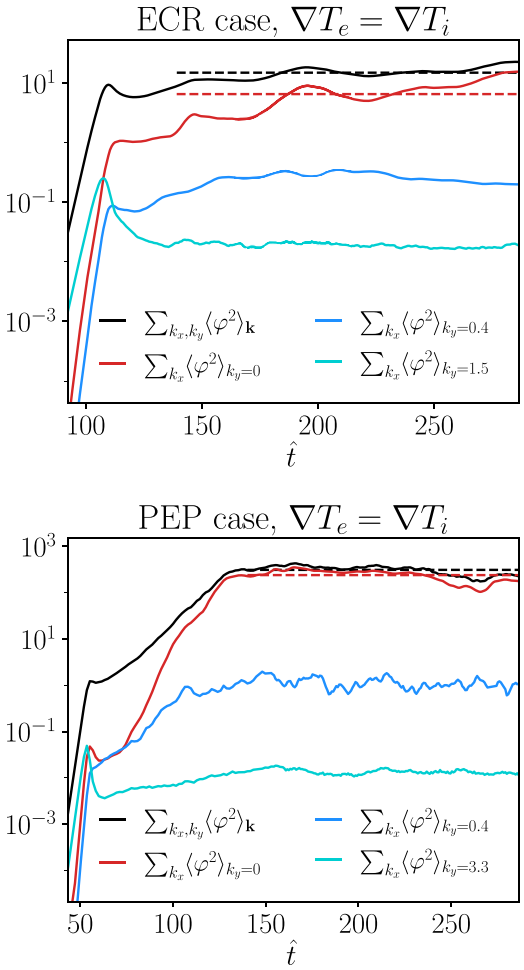

FIG. 4. Time traces for linear dominant and zonal modes ($k_y = 0$), nonlinearly dominant modes ($k_y\rho_i = 0.4$), and all evolving scales.

suppression due to density peaking, like the one reported in Ref. [5]. Instead, a partial turbulence suppression must be ascribed to a violent growth of the zonal flow, which reaches larger amplitudes than for moderate density gradients. Interestingly, at the ion scale, electron heat transport can be dominant.

A quantitative comparison of numerical and experimental suppression of turbulence in W7-X remains unsatisfactory and challenging, but not out of reach, and will likely involve considering electromagnetic, collisional and radially global effects, which will be addressed in a future publication. Very encouragingly, preliminary experimental results are in accordance with our theoretical predictions [25].

ACKNOWLEDGMENTS

We are grateful to P. Helander, M. Barnes, E. Rodriguez, G. Merlo, and A. Di Siena for insightful discussions. Simulations were performed with the HPCs Raven (Garching) and Marconi (Casalecchio di Reno, Bologna). This work has been carried out within the framework of the EUROfusion Consortium, funded by the European Union via the Euratom Research and Training Programme under Grant Agreement No. 101052200-EUROfusion. The views and opinions

expressed are, however, those of the authors only and do not necessarily reflect those of the European Union or the European Commission. Neither the European Union nor the European Commission can be held responsible for them.

[1] T. Klinger, A. Alonso, S. Bozhenkov, R. Burhenn, A. Dinklage, G. Fuchert, J. Geiger, O. Grulke, A. Langenberg, M. Hirsch, G. Kocsis, J. Knauer, A. Krämer-Flecken, H. Laqua, S. Lazerson, M. Landreman, H. Maaßberg, S. Marsen, M. Otte, N. Pablant *et al.*, Performance and properties of the first plasmas of Wendelstein 7-X, Plasma Phys. Control. Fusion **59**, 014018 (2017).

[2] A. Dinklage, C. Beidler, and the Wendelstein 7-X team, Magnetic configuration effects on the Wendelstein 7-X stellarator, Nat. Phys. **14**, 855 (2018).

[3] C. D. Beidler, Smith, A. H. M. Alonso, T. Andreeva, J. Baldzuhn, M. N. A. Beurskens, M. Borchardt, S. A. Bozhenkov, K. J. Brunner, H. Damm, M. Drevlak, O. P. Ford, G. Fuchert, J. Geiger, P. Helander, U. Hergenhahn, M. Hirsch, U. Höfel, Y. O. Kazakov, R. Kleiber *et al.*, Demonstration of reduced neoclassical energy transport in Wendelstein 7-X, Nature (London) **596**, 221 (2021).

[4] S. Bozhenkov, Y. Kazakov, O. Ford, M. Beurskens, J. Alcusón, J. Alonso, J. Baldzuhn, C. Brandt, K. Brunner, H. Damm, G. Fuchert, J. Geiger, O. Grulke, M. Hirsch, U. Höfel, Z. Huang, J. Knauer, M. Krychowiak, A. Langenberg, H. Laqua *et al.*, High-performance plasmas after pellet injections in Wendelstein 7-X, Nucl. Fusion **60**, 066011 (2020).

[5] P. Xanthopoulos, S. A. Bozhenkov, M. N. Beurskens, H. M. Smith, G. G. Plunk, P. Helander, C. D. Beidler, J. A. Alcusón, A. Alonso, A. Dinklage, O. Ford, G. Fuchert, J. Geiger, J. H. E. Proll, M. J. Pueschel, Y. Turkin, and F. Warmer (The W7-X Team), Turbulence mechanisms of enhanced performance stellarator plasmas, Phys. Rev. Lett. **125**, 075001 (2020).

[6] F. Wilms, A. B. Navarro, T. Windisch, S. Bozhenkov, F. Warmer, G. Fuchert, O. Ford, D. Zhang, T. Stange, and F. Jenko (The W7-X Team), Global gyrokinetic analysis of Wendelstein 7-X discharge: Unveiling the importance of trapped-electron-mode and electron-temperature-gradient turbulence, arXiv:2402.14403.

[7] F. Wilms, A. Banon Navarro, and F. Jenko, Full-flux-surface effects on electrostatic turbulence in Wendelstein 7-X-like plasmas, Nucl. Fusion **63**, 086004 (2023).

[8] P. Helander and A. Zocco, Quasilinear particle transport from gyrokinetic instabilities in general magnetic geometry, Plasma Phys. Control. Fusion **60**, 084006 (2018).

[9] H. Thienpondt, J. M. García-Regaña, I. Calvo, J. A. Alonso, J. L. Velasco, A. González-Jerez, M. Barnes, K. Brunner, O. Ford, G. Fuchert, J. Knauer, E. Pasch, and L. Vanó (The Wendelstein 7-X Team), Prevention of core particle depletion in stellarators by turbulence, Phys. Rev. Res. **5**, L022053 (2023).

[10] M. Barnes, F. Parra, and M. Landreman, STELLA: An operator-split, implicit–explicit δf-gyrokinetic code for general magnetic field configurations, J. Comput. Phys. **391**, 365 (2019).

[11] F. Jenko, W. Dorland, M. Kotschenreuther, and B. N. Rogers, Electron temperature gradient driven turbulence, Phys. Plasmas **7**, 1904 (2000).

[12] E. A. Frieman and L. Chen, Nonlinear gyrokinetic equations for low-frequency electromagnetic waves in general plasma equilibria, Phys. Fluids **25**, 502 (1982).

[13] B. Coppi and F. Pegoraro, Theory of the ubiquitous mode, Nucl. Fusion **17**, 969 (1977).

[14] G. G. Plunk, J. W. Connor, and P. Helander, Collisionless microinstabilities in stellarators. Part 4. The ion-driven trapped-electron mode, J. Plasma Phys. **83**, 715830404 (2017).

[15] J. Chowdhury, R. Ganesh, S. Brunner, J. Vaclavik, and L. Villard, Toroidal universal drift instability: A global gyrokinetic study, Phys. Plasmas **17**, 102105 (2010).

[16] P. Helander and G. G. Plunk, The universal instability in general geometry, Phys. Plasmas **22**, 090706 (2015).

[17] L. Podavini, A. Zocco, J. M. García-Regaña, M. Barnes, F. I. Parra, A. Mishchenko, and P. Helander, Electrostatic microinstabilities and turbulence in Wendelstein 7-X close to the stability threshold, arXiv:2311.04342.

[18] Z. Gao, H. Sanuki, K. Itoh, and J. Q. Dong, Short wavelength ion temperature gradient instability in toroidal plasmas, Phys. Plasmas **12**, 022502 (2005).

[19] J. Chowdhury, S. Brunner, R. Ganesh, X. Lapillonne, L. Villard, and F. Jenko, Short wavelength ion temperature gradient turbulence, Phys. Plasmas **19**, 102508 (2012).

[20] E. Rodriguez and A. Zocco, The ion-temperature-gradient-driven mode and its localisation, J. Plasma Phys. (to be published).

[21] E. Sánchez, J. García-Regaña, A. B. Navarro, J. Proll, C. M. Moreno, A. González-Jerez, I. Calvo, R. Kleiber, J. Riemann, J. Smoniewski, M. Barnes, and F. Parra, Gyrokinetic simulations in stellarators using different computational domains, Nucl. Fusion **61**, 116074 (2021).

[22] T. Görler and F. Jenko, Scale separation between electron and ion thermal transport, Phys. Rev. Lett. **100**, 185002 (2008).

[23] S. Maeyama, Y. Idomura, T. H. Watanabe, M. Nakata, M. Yagi, N. Miyato, A. Ishizawa, and M. Nunami, Cross-scale interactions between electron and ion scale turbulence in a tokamak plasma, Phys. Rev. Lett. **114**, 255002 (2015).

[24] N. Howard, C. Holland, A. White, M. Greenwald, and J. Candy, Multi-scale gyrokinetic simulation of tokamak plasmas: Enhanced heat loss due to cross-scale coupling of plasma turbulence, Nucl. Fusion **56**, 014004 (2016).

[25] G. Weir (Private Communication).